BABAR-CONF-06/40
SLAC-PUB-12015
hep-ex/0607112

Measurement of *CP*-Violating Asymmetries in the $B^0 \rightarrow K^+K^-K^0$ Dalitz Plot

The *BABAR* Collaboration

July 31, 2006

Abstract

We present a preliminary measurement of *CP*-violation parameters in the decay $B^0 \rightarrow K^+K^-K^0$, using approximately 347 million $B\overline{B}$ events collected by the *BABAR* detector at SLAC. Reconstructing the neutral kaon as $K^0_S \rightarrow \pi^+\pi^-, K^0_S \rightarrow \pi^0\pi^0$, or K^0_L, we analyze the Dalitz plot distribution and measure fractions to intermediate states. We extract *CP* parameters from the asymmetries in amplitudes and phases between B^0 and $\overline{B}^0$ decays across the Dalitz plot. For decays to ϕK^0, we find $\beta_{\mathit{eff}} = 0.06 \pm 0.16 \pm 0.05$, $A_{CP} = -0.18 \pm 0.20 \pm 0.10$, where the first uncertainty is statistical and the second one is systematic. For decays to f_0K^0, we find $\beta_{\mathit{eff}} = 0.18 \pm 0.19 \pm 0.04$, $A_{CP} = 0.45 \pm 0.28 \pm 0.10$. Combining all $K^+K^-K^0$ events and taking account of the different *CP* eigenvalues of the individual Dalitz plot components, we find $\beta_{\mathit{eff}} = 0.361 \pm 0.079 \pm 0.037$, $A_{CP} = -0.034 \pm 0.079 \pm 0.025$. The trigonometric reflection at $\pi/2 - \beta_{\mathit{eff}}$ is disfavored at 4.6σ. We also study angular distributions in $B^0 \rightarrow K^+K^-K^0_S$ and $B^+ \rightarrow \phi K^+$ decays and measure the direct *CP* asymmetry in $B^+ \rightarrow \phi K^+$ decays, $A_{CP} = 0.046 \pm 0.046 \pm 0.017$.

Submitted to the 33$^{\text{rd}}$ International Conference on High-Energy Physics, ICHEP 06,
26 July—2 August 2006, Moscow, Russia.

Stanford Linear Accelerator Center, Stanford University, Stanford, CA 94309

Work supported in part by Department of Energy contract DE-AC02-76SF00515.

The *BABAR* Collaboration,

B. Aubert, R. Barate, M. Bona, D. Boutigny, F. Couderc, Y. Karyotakis, J. P. Lees, V. Poireau, V. Tisserand, A. Zghiche

Laboratoire de Physique des Particules, IN2P3/CNRS et Université de Savoie, F-74941 Annecy-Le-Vieux, France

E. Grauges

Universitat de Barcelona, Facultat de Fisica, Departament ECM, E-08028 Barcelona, Spain

A. Palano

Università di Bari, Dipartimento di Fisica and INFN, I-70126 Bari, Italy

J. C. Chen, N. D. Qi, G. Rong, P. Wang, Y. S. Zhu

Institute of High Energy Physics, Beijing 100039, China

G. Eigen, I. Ofte, B. Stugu

University of Bergen, Institute of Physics, N-5007 Bergen, Norway

G. S. Abrams, M. Battaglia, D. N. Brown, J. Button-Shafer, R. N. Cahn, E. Charles, M. S. Gill, Y. Groysman, R. G. Jacobsen, J. A. Kadyk, L. T. Kerth, Yu. G. Kolomensky, G. Kukartsev, G. Lynch, L. M. Mir, T. J. Orimoto, M. Pripstein, N. A. Roe, M. T. Ronan, W. A. Wenzel

Lawrence Berkeley National Laboratory and University of California, Berkeley, California 94720, USA

P. del Amo Sanchez, M. Barrett, K. E. Ford, A. J. Hart, T. J. Harrison, C. M. Hawkes, S. E. Morgan, A. T. Watson

University of Birmingham, Birmingham, B15 2TT, United Kingdom

T. Held, H. Koch, B. Lewandowski, M. Pelizaeus, K. Peters, T. Schroeder, M. Steinke

Ruhr Universität Bochum, Institut für Experimentalphysik 1, D-44780 Bochum, Germany

J. T. Boyd, J. P. Burke, W. N. Cottingham, D. Walker

University of Bristol, Bristol BS8 1TL, United Kingdom

D. J. Asgeirsson, T. Cuhadar-Donszelmann, B. G. Fulsom, C. Hearty, N. S. Knecht, T. S. Mattison, J. A. McKenna

University of British Columbia, Vancouver, British Columbia, Canada V6T 1Z1

A. Khan, P. Kyberd, M. Saleem, D. J. Sherwood, L. Teodorescu

Brunel University, Uxbridge, Middlesex UB8 3PH, United Kingdom

V. E. Blinov, A. D. Bukin, V. P. Druzhinin, V. B. Golubev, A. P. Onuchin, S. I. Serednyakov, Yu. I. Skovpen, E. P. Solodov, K. Yu Todyshev

Budker Institute of Nuclear Physics, Novosibirsk 630090, Russia

D. S. Best, M. Bondioli, M. Bruinsma, M. Chao, S. Curry, I. Eschrich, D. Kirkby, A. J. Lankford, P. Lund, M. Mandelkern, R. K. Mommsen, W. Roethel, D. P. Stoker

University of California at Irvine, Irvine, California 92697, USA

S. Abachi, C. Buchanan

University of California at Los Angeles, Los Angeles, California 90024, USA

S. D. Foulkes, J. W. Gary, O. Long, B. C. Shen, K. Wang, L. Zhang
University of California at Riverside, Riverside, California 92521, USA

H. K. Hadavand, E. J. Hill, H. P. Paar, S. Rahatlou, V. Sharma
University of California at San Diego, La Jolla, California 92093, USA

J. W. Berryhill, C. Campagnari, A. Cunha, B. Dahmes, T. M. Hong, D. Kovalskyi, J. D. Richman
University of California at Santa Barbara, Santa Barbara, California 93106, USA

T. W. Beck, A. M. Eisner, C. J. Flacco, C. A. Heusch, J. Kroseberg, W. S. Lockman, G. Nesom, T. Schalk, B. A. Schumm, A. Seiden, P. Spradlin, D. C. Williams, M. G. Wilson
University of California at Santa Cruz, Institute for Particle Physics, Santa Cruz, California 95064, USA

J. Albert, E. Chen, A. Dvoretskii, F. Fang, D. G. Hitlin, I. Narsky, T. Piatenko, F. C. Porter, A. Ryd, A. Samuel
California Institute of Technology, Pasadena, California 91125, USA

G. Mancinelli, B. T. Meadows, K. Mishra, M. D. Sokoloff
University of Cincinnati, Cincinnati, Ohio 45221, USA

F. Blanc, P. C. Bloom, S. Chen, W. T. Ford, J. F. Hirschauer, A. Kreisel, M. Nagel, U. Nauenberg, A. Olivas, W. O. Ruddick, J. G. Smith, K. A. Ulmer, S. R. Wagner, J. Zhang
University of Colorado, Boulder, Colorado 80309, USA

A. Chen, E. A. Eckhart, A. Soffer, W. H. Toki, R. J. Wilson, F. Winklmeier, Q. Zeng
Colorado State University, Fort Collins, Colorado 80523, USA

D. D. Altenburg, E. Feltresi, A. Hauke, H. Jasper, J. Merkel, A. Petzold, B. Spaan
Universität Dortmund, Institut für Physik, D-44221 Dortmund, Germany

T. Brandt, V. Klose, H. M. Lacker, W. F. Mader, R. Nogowski, J. Schubert, K. R. Schubert, R. Schwierz, J. E. Sundermann, A. Volk
Technische Universität Dresden, Institut für Kern- und Teilchenphysik, D-01062 Dresden, Germany

D. Bernard, G. R. Bonneaud, E. Latour, Ch. Thiebaux, M. Verderi
Laboratoire Leprince-Ringuet, CNRS/IN2P3, Ecole Polytechnique, F-91128 Palaiseau, France

P. J. Clark, W. Gradl, F. Muheim, S. Playfer, A. I. Robertson, Y. Xie
University of Edinburgh, Edinburgh EH9 3JZ, United Kingdom

M. Andreotti, D. Bettoni, C. Bozzi, R. Calabrese, G. Cibinetto, E. Luppi, M. Negrini, A. Petrella, L. Piemontese, E. Prencipe
Università di Ferrara, Dipartimento di Fisica and INFN, I-44100 Ferrara, Italy

F. Anulli, R. Baldini-Ferroli, A. Calcaterra, R. de Sangro, G. Finocchiaro, S. Pacetti, P. Patteri, I. M. Peruzzi,[1] M. Piccolo, M. Rama, A. Zallo
Laboratori Nazionali di Frascati dell'INFN, I-00044 Frascati, Italy

[1]Also with Università di Perugia, Dipartimento di Fisica, Perugia, Italy

A. Buzzo, R. Capra, R. Contri, M. Lo Vetere, M. M. Macri, M. R. Monge, S. Passaggio, C. Patrignani, E. Robutti, A. Santroni, S. Tosi

Università di Genova, Dipartimento di Fisica and INFN, I-16146 Genova, Italy

G. Brandenburg, K. S. Chaisanguanthum, M. Morii, J. Wu

Harvard University, Cambridge, Massachusetts 02138, USA

R. S. Dubitzky, J. Marks, S. Schenk, U. Uwer

Universität Heidelberg, Physikalisches Institut, Philosophenweg 12, D-69120 Heidelberg, Germany

D. J. Bard, W. Bhimji, D. A. Bowerman, P. D. Dauncey, U. Egede, R. L. Flack, J. A. Nash, M. B. Nikolich, W. Panduro Vazquez

Imperial College London, London, SW7 2AZ, United Kingdom

P. K. Behera, X. Chai, M. J. Charles, U. Mallik, N. T. Meyer, V. Ziegler

University of Iowa, Iowa City, Iowa 52242, USA

J. Cochran, H. B. Crawley, L. Dong, V. Eyges, W. T. Meyer, S. Prell, E. I. Rosenberg, A. E. Rubin

Iowa State University, Ames, Iowa 50011-3160, USA

A. V. Gritsan

Johns Hopkins University, Baltimore, Maryland 21218, USA

A. G. Denig, M. Fritsch, G. Schott

Universität Karlsruhe, Institut für Experimentelle Kernphysik, D-76021 Karlsruhe, Germany

N. Arnaud, M. Davier, G. Grosdidier, A. Höcker, F. Le Diberder, V. Lepeltier, A. M. Lutz, A. Oyanguren, S. Pruvot, S. Rodier, P. Roudeau, M. H. Schune, A. Stocchi, W. F. Wang, G. Wormser

Laboratoire de l'Accélérateur Linéaire, IN2P3/CNRS et Université Paris-Sud 11, Centre Scientifique d'Orsay, B.P. 34, F-91898 ORSAY Cedex, France

C. H. Cheng, D. J. Lange, D. M. Wright

Lawrence Livermore National Laboratory, Livermore, California 94550, USA

C. A. Chavez, I. J. Forster, J. R. Fry, E. Gabathuler, R. Gamet, K. A. George, D. E. Hutchcroft, D. J. Payne, K. C. Schofield, C. Touramanis

University of Liverpool, Liverpool L69 7ZE, United Kingdom

A. J. Bevan, F. Di Lodovico, W. Menges, R. Sacco

Queen Mary, University of London, E1 4NS, United Kingdom

G. Cowan, H. U. Flaecher, D. A. Hopkins, P. S. Jackson, T. R. McMahon, S. Ricciardi, F. Salvatore, A. C. Wren

University of London, Royal Holloway and Bedford New College, Egham, Surrey TW20 0EX, United Kingdom

D. N. Brown, C. L. Davis

University of Louisville, Louisville, Kentucky 40292, USA

J. Allison, N. R. Barlow, R. J. Barlow, Y. M. Chia, C. L. Edgar, G. D. Lafferty, M. T. Naisbit, J. C. Williams, J. I. Yi

University of Manchester, Manchester M13 9PL, United Kingdom

C. Chen, W. D. Hulsbergen, A. Jawahery, C. K. Lae, D. A. Roberts, G. Simi

University of Maryland, College Park, Maryland 20742, USA

G. Blaylock, C. Dallapiccola, S. S. Hertzbach, X. Li, T. B. Moore, S. Saremi, H. Staengle

University of Massachusetts, Amherst, Massachusetts 01003, USA

R. Cowan, G. Sciolla, S. J. Sekula, M. Spitznagel, F. Taylor, R. K. Yamamoto

Massachusetts Institute of Technology, Laboratory for Nuclear Science, Cambridge, Massachusetts 02139, USA

H. Kim, S. E. Mclachlin, P. M. Patel, S. H. Robertson

McGill University, Montréal, Québec, Canada H3A 2T8

A. Lazzaro, V. Lombardo, F. Palombo

Università di Milano, Dipartimento di Fisica and INFN, I-20133 Milano, Italy

J. M. Bauer, L. Cremaldi, V. Eschenburg, R. Godang, R. Kroeger, D. A. Sanders, D. J. Summers, H. W. Zhao

University of Mississippi, University, Mississippi 38677, USA

S. Brunet, D. Côté, M. Simard, P. Taras, F. B. Viaud

Université de Montréal, Physique des Particules, Montréal, Québec, Canada H3C 3J7

H. Nicholson

Mount Holyoke College, South Hadley, Massachusetts 01075, USA

N. Cavallo,[2] G. De Nardo, F. Fabozzi,[3] C. Gatto, L. Lista, D. Monorchio, P. Paolucci, D. Piccolo, C. Sciacca

Università di Napoli Federico II, Dipartimento di Scienze Fisiche and INFN, I-80126, Napoli, Italy

M. A. Baak, G. Raven, H. L. Snoek

NIKHEF, National Institute for Nuclear Physics and High Energy Physics, NL-1009 DB Amsterdam, The Netherlands

C. P. Jessop, J. M. LoSecco

University of Notre Dame, Notre Dame, Indiana 46556, USA

T. Allmendinger, G. Benelli, L. A. Corwin, K. K. Gan, K. Honscheid, D. Hufnagel, P. D. Jackson, H. Kagan, R. Kass, A. M. Rahimi, J. J. Regensburger, R. Ter-Antonyan, Q. K. Wong

Ohio State University, Columbus, Ohio 43210, USA

N. L. Blount, J. Brau, R. Frey, O. Igonkina, J. A. Kolb, M. Lu, R. Rahmat, N. B. Sinev, D. Strom, J. Strube, E. Torrence

University of Oregon, Eugene, Oregon 97403, USA

[2]Also with Università della Basilicata, Potenza, Italy

[3]Also with Università della Basilicata, Potenza, Italy

A. Gaz, M. Margoni, M. Morandin, A. Pompili, M. Posocco, M. Rotondo, F. Simonetto, R. Stroili, C. Voci
Università di Padova, Dipartimento di Fisica and INFN, I-35131 Padova, Italy

M. Benayoun, H. Briand, J. Chauveau, P. David, L. Del Buono, Ch. de la Vaissière, O. Hamon, B. L. Hartfiel, M. J. J. John, Ph. Leruste, J. Malclès, J. Ocariz, L. Roos, G. Therin
Laboratoire de Physique Nucléaire et de Hautes Energies, IN2P3/CNRS, Université Pierre et Marie Curie-Paris6, Université Denis Diderot-Paris7, F-75252 Paris, France

L. Gladney, J. Panetta
University of Pennsylvania, Philadelphia, Pennsylvania 19104, USA

M. Biasini, R. Covarelli
Università di Perugia, Dipartimento di Fisica and INFN, I-06100 Perugia, Italy

C. Angelini, G. Batignani, S. Bettarini, F. Bucci, G. Calderini, M. Carpinelli, R. Cenci, F. Forti, M. A. Giorgi, A. Lusiani, G. Marchiori, M. A. Mazur, M. Morganti, N. Neri, E. Paoloni, G. Rizzo, J. J. Walsh
Università di Pisa, Dipartimento di Fisica, Scuola Normale Superiore and INFN, I-56127 Pisa, Italy

M. Haire, D. Judd, D. E. Wagoner
Prairie View A&M University, Prairie View, Texas 77446, USA

J. Biesiada, N. Danielson, P. Elmer, Y. P. Lau, C. Lu, J. Olsen, A. J. S. Smith, A. V. Telnov
Princeton University, Princeton, New Jersey 08544, USA

F. Bellini, G. Cavoto, A. D'Orazio, D. del Re, E. Di Marco, R. Faccini, F. Ferrarotto, F. Ferroni, M. Gaspero, L. Li Gioi, M. A. Mazzoni, S. Morganti, G. Piredda, F. Polci, F. Safai Tehrani, C. Voena
Università di Roma La Sapienza, Dipartimento di Fisica and INFN, I-00185 Roma, Italy

M. Ebert, H. Schröder, R. Waldi
Universität Rostock, D-18051 Rostock, Germany

T. Adye, N. De Groot, B. Franek, E. O. Olaiya, F. F. Wilson
Rutherford Appleton Laboratory, Chilton, Didcot, Oxon, OX11 0QX, United Kingdom

R. Aleksan, S. Emery, A. Gaidot, S. F. Ganzhur, G. Hamel de Monchenault, W. Kozanecki, M. Legendre, G. Vasseur, Ch. Yèche, M. Zito
DSM/Dapnia, CEA/Saclay, F-91191 Gif-sur-Yvette, France

X. R. Chen, H. Liu, W. Park, M. V. Purohit, J. R. Wilson
University of South Carolina, Columbia, South Carolina 29208, USA

M. T. Allen, D. Aston, R. Bartoldus, P. Bechtle, N. Berger, R. Claus, J. P. Coleman, M. R. Convery, M. Cristinziani, J. C. Dingfelder, J. Dorfan, G. P. Dubois-Felsmann, D. Dujmic, W. Dunwoodie, R. C. Field, T. Glanzman, S. J. Gowdy, M. T. Graham, P. Grenier,[4] V. Halyo, C. Hast, T. Hryn'ova, W. R. Innes, M. H. Kelsey, P. Kim, D. W. G. S. Leith, S. Li, S. Luitz, V. Luth, H. L. Lynch, D. B. MacFarlane, H. Marsiske, R. Messner, D. R. Muller, C. P. O'Grady, V. E. Ozcan, A. Perazzo, M. Perl, T. Pulliam, B. N. Ratcliff, A. Roodman, A. A. Salnikov, R. H. Schindler, J. Schwiening, A. Snyder, J. Stelzer, D. Su, M. K. Sullivan, K. Suzuki, S. K. Swain, J. M. Thompson, J. Va'vra, N. van

[4]Also at Laboratoire de Physique Corpusculaire, Clermont-Ferrand, France

Bakel, M. Weaver, A. J. R. Weinstein, W. J. Wisniewski, M. Wittgen, D. H. Wright, A. K. Yarritu, K. Yi, C. C. Young

Stanford Linear Accelerator Center, Stanford, California 94309, USA

P. R. Burchat, A. J. Edwards, S. A. Majewski, B. A. Petersen, C. Roat, L. Wilden

Stanford University, Stanford, California 94305-4060, USA

S. Ahmed, M. S. Alam, R. Bula, J. A. Ernst, V. Jain, B. Pan, M. A. Saeed, F. R. Wappler, S. B. Zain

State University of New York, Albany, New York 12222, USA

W. Bugg, M. Krishnamurthy, S. M. Spanier

University of Tennessee, Knoxville, Tennessee 37996, USA

R. Eckmann, J. L. Ritchie, A. Satpathy, C. J. Schilling, R. F. Schwitters

University of Texas at Austin, Austin, Texas 78712, USA

J. M. Izen, X. C. Lou, S. Ye

University of Texas at Dallas, Richardson, Texas 75083, USA

F. Bianchi, F. Gallo, D. Gamba

Università di Torino, Dipartimento di Fisica Sperimentale and INFN, I-10125 Torino, Italy

M. Bomben, L. Bosisio, C. Cartaro, F. Cossutti, G. Della Ricca, S. Dittongo, L. Lanceri, L. Vitale

Università di Trieste, Dipartimento di Fisica and INFN, I-34127 Trieste, Italy

V. Azzolini, N. Lopez-March, F. Martinez-Vidal

IFIC, Universitat de Valencia-CSIC, E-46071 Valencia, Spain

Sw. Banerjee, B. Bhuyan, C. M. Brown, D. Fortin, K. Hamano, R. Kowalewski, I. M. Nugent, J. M. Roney, R. J. Sobie

University of Victoria, Victoria, British Columbia, Canada V8W 3P6

J. J. Back, P. F. Harrison, T. E. Latham, G. B. Mohanty, M. Pappagallo

Department of Physics, University of Warwick, Coventry CV4 7AL, United Kingdom

H. R. Band, X. Chen, B. Cheng, S. Dasu, M. Datta, K. T. Flood, J. J. Hollar, P. E. Kutter, B. Mellado, A. Mihalyi, Y. Pan, M. Pierini, R. Prepost, S. L. Wu, Z. Yu

University of Wisconsin, Madison, Wisconsin 53706, USA

H. Neal

Yale University, New Haven, Connecticut 06511, USA

1 INTRODUCTION

We describe a B-flavor tagged, time-dependent Dalitz plot analysis of the $B^0 \to K^+K^-K^0$ decay [1], with the K^0 reconstructed as $K^0_S \to \pi^+\pi^-$, $K^0_S \to \pi^0\pi^0$, or K^0_L. In the Standard Model (SM), these decays are dominated by $b \to s\bar{s}s$ gluonic penguin amplitudes, with a single weak phase. Contributions from $b \to u\bar{q}q$ tree amplitudes, proportional to the Cabibbo-Kobayashi-Maskawa (CKM) matrix element V_{ub} with a *CP*-violating weak phase γ [2], are small, but may depend on the position in the Dalitz plot. In $B^0 \to \phi(K^+K^-)K^0$ decays the modification of the *CP* asymmetry due to the presence of suppressed tree amplitudes is at $\mathcal{O}(0.01)$ [3, 4], while at higher K^+K^- masses a larger contribution at $\mathcal{O}(0.1)$ is possible [5]. Therefore, to very good precision, we also expect the direct *CP* asymmetry for these decays to be small in the SM. The *CP* asymmetry in $B^0 \to K^+K^-K^0$ decay arises from the interference of decays and $B^0 \leftrightarrow \overline{B}^0$ mixing, with a relative phase of 2β. The Unitarity Triangle angle β has been measured in $B^0 \to [c\bar{c}]K^0$ decays to be $\sin 2\beta = 0.685 \pm 0.032$ [6, 7]. Current direct measurements favor the solution of $\beta = 0.37$ over $\beta = 1.20$ at the 98.3% C.L. [8].

The decay $B^0 \to K^+K^-K^0$ is one of the most promising processes with which to search for physics beyond the SM. Since the leading amplitudes enter only at the one-loop level, additional contributions from heavy non-SM particles may be of comparable size. If the amplitude from heavy particles has a *CP*-violating phase, the measured *CP*-violation parameters may differ from those expected in the SM.

Previous measurements of the *CP* asymmetry in $B^0 \to K^+K^-K^0$ decays have been performed separately around the ϕ mass, and for higher K^+K^- masses, neglecting interference effects between intermediate states [9]. In this analysis, we extract the *CP*-violation parameters by taking into account different amplitudes and phases across the B^0 and $\overline{B}^0$ Dalitz plots.

2 EVENT RECONSTRUCTION

The data used in this analysis were collected with the *BABAR* detector at the PEP-II asymmetric-energy B factory at SLAC. A total of 347 million $B\overline{B}$ pairs were used.

The *BABAR* detector is described in detail elsewhere [10]. Charged particle (track) momenta are measured with a 5-layer double-sided silicon vertex tracker (SVT) and a 40-layer drift chamber (DCH) coaxial with a 1.5-T superconducting solenoidal magnet. Neutral cluster (photon) positions and energies are measured with an electromagnetic calorimeter (EMC) consisting of 6580 CsI(Tl) crystals. Charged hadrons are identified with a detector of internally reflected Cherenkov light (DIRC) and specific ionization measurements ($\mathrm{d}E/\mathrm{d}x$) in the tracking detectors (DCH, SVT). Neutral hadrons that do not interact in the EMC are identified with detectors, up to 15 layers deep, in the flux return steel (IFR).

We reconstruct $B^0 \to K^+K^-K^0$ decays by combining two oppositely charged tracks with a $K^0_S \to \pi^+\pi^-$, $K^0_S \to \pi^0\pi^0$, or K^0_L candidate. $B^+ \to \phi K^+$ decays are reconstructed from three charged tracks. The K^+ and K^- tracks must have at least 12 measured DCH coordinates, a minimum transverse momentum of 0.1 GeV/c, and must originate from the nominal beam spot. Tracks are identified as kaons using a likelihood ratio that combines $\mathrm{d}E/\mathrm{d}x$ measured in the SVT and DCH with the Cherenkov angle and number of photons measured in the DIRC. For K^+K^- masses near the ϕ mass, higher efficiency kaon identification is used, while for higher masses higher purity criteria are chosen to reduce background.

For all modes, the main background is from random combinations of particles produced in events of the type $e^+e^- \to q\bar{q}$ ($q = u, d, s, c$) (continuum). Additional background from decays of B mesons to other final states, with and without charm particles, is estimated from Monte Carlo simulation.

We use event-shape variables, computed in the center-of-mass (CM) frame, to separate continuum events with a jet-like topology from the more isotropic B decays. Continuum events are suppressed with a requirement on the quantity $\cos(\theta_{\rm T})$, $\cos(\theta_{\rm T}) < 0.9$, where $\theta_{\rm T}$ is the angle between the thrust axis of the B candidate's daughters and the thrust axis formed from the other charged and neutral particles in the event. We select events in the range . Further discrimination comes from the Legendre moments $\mathcal{L}_{i=0,2} = \sum_j p_j L_i(\theta_j)$, where the sum is over all tracks and clusters not used to reconstruct the B meson; L_i is the Legendre polynomial of order i, and θ_j is the angle to the B thrust axis. Lastly, the magnitude of the cosine of the angle of the B with respect to the collision axis $|\cos\theta_B|$, is also used.

2.1 $B^0 \to K^+K^-K^0_S$, $K^0_S \to \pi^+\pi^-$

For decays $B^0 \to K^+K^-K^0_S$ and $K^0_S \to \pi^+\pi^-$, K^0_S candidates are formed from oppositely charged tracks with an invariant mass within 20 MeV/c^2 of the K^0_S mass [2]. The K^0_S vertex is required to be separated from the B^0 vertex by at least 3σ. The angle α between the K^0_S momentum vector and the vector connecting the B^0 and K^0_S vertices must satisfy $\cos\alpha > 0.999$.

B candidates are identified using two kinematic variables that separate signal from continuum background. These are the beam-energy-substituted mass $m_{\rm ES} = \sqrt{(s/2 + \mathbf{p}_i \cdot \mathbf{p}_B)^2/E_i^2 - \mathbf{p}_B^2}$, where $\sqrt{s}$ is the total e^+e^- CM (CM) energy, $(E_i, \mathbf{p}_i)$ is the four-momentum of the initial e^+e^- system and $\mathbf{p}_B$ is the B candidate momentum, both measured in the laboratory frame, and $\Delta E = E_B - \sqrt{s}/2$, where E_B is the B candidate energy in the CM frame. Distributions of these variables in data, for signal and background events calculated using the ${}_s\mathcal{P}lot$ event-weighting technique [11], are shown in Fig. 1.

2.2 $B^0 \to K^+K^-K^0_S$, $K^0_S \to \pi^0\pi^0$

For decays $B^0 \to K^+K^-K^0_S$ and $K^0_S \to \pi^0\pi^0$, K^0_S candidates are formed from two $\pi^0 \to \gamma\gamma$ candidates. Each of the four photons must have $E_\gamma > 0.05\,\mathrm{GeV}$ and have a transverse shower shape loosely consistent with an electromagnetic shower. Additionally, we require each π^0 candidate to satisfy $0.100 < m_{\gamma\gamma} < 0.155\,\mathrm{GeV}/c^2$. The resulting $K^0_S \to \pi^0\pi^0$ mass is required to satisfy $0.4776 < m_{\pi^0\pi^0} < 0.5276$ GeV/c^2. A K^0_S mass constraint is then applied for the reconstruction of the B^0 candidate.

The kinematic variables $m_{\rm ES}$ and ΔE are formed for each candidate as in Sec. 2.1. Distributions of these variables are shown in Fig. 2. Note that the mean of the signal ΔE distribution is shifted from zero due to energy leakage in the EMC.

2.3 $B^0 \to K^+K^-K^0_L$

We identify a K^0_L candidate either as a cluster of energy deposited in the EMC or as a cluster of hits in two or more layers of the IFR that cannot be associated with any charged track in the event. The K^0_L energy is not measured. Therefore, we determine the K^0_L laboratory momentum from its flight direction as measured from the EMC or IFR cluster, and the constraint that the invariant $K^+K^-K^0_L$ mass equal the B^0 mass [2]. In those cases where the K^0_L is detected in both the IFR and EMC we use the angular information from the EMC, because it has higher precision. In

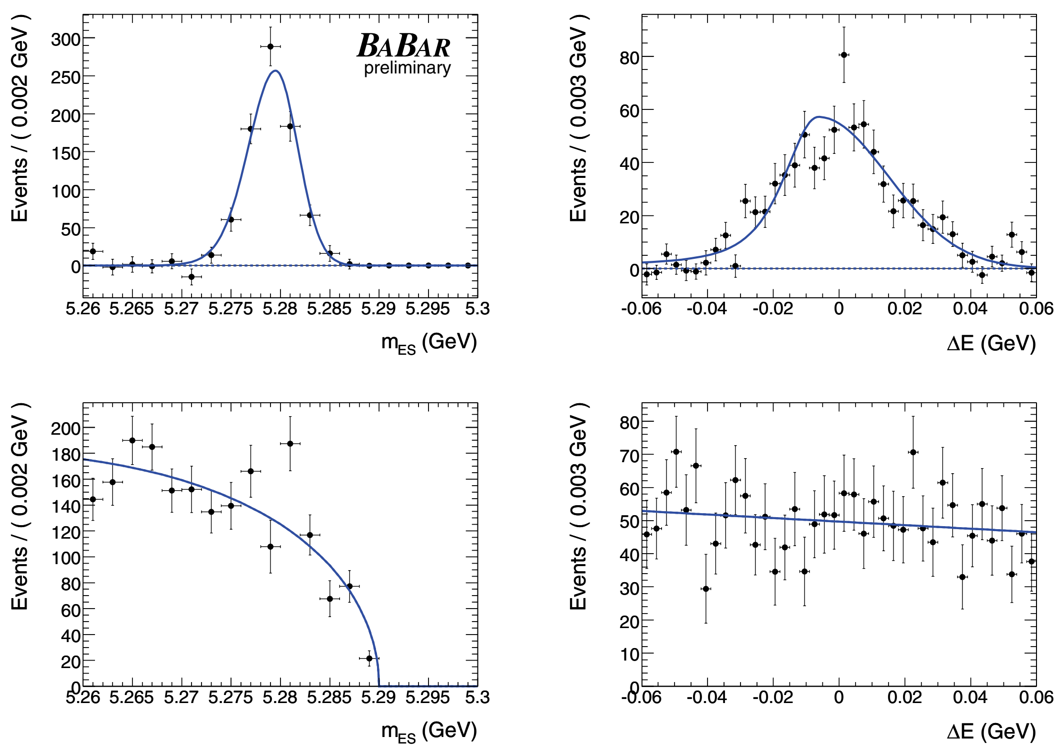

Figure 1: Distributions of kinematic variables (left) m_{ES} and (right) ΔE for the $K^+K^-K^0_S(\pi^+\pi^-)$ subsample: (top) signal, (bottom) continuum background. The points are data events weighted with the ${}_s\mathcal{P}lot$ technique [11], and the curves are the PDF shapes used in the ML fit (Sec. 3).

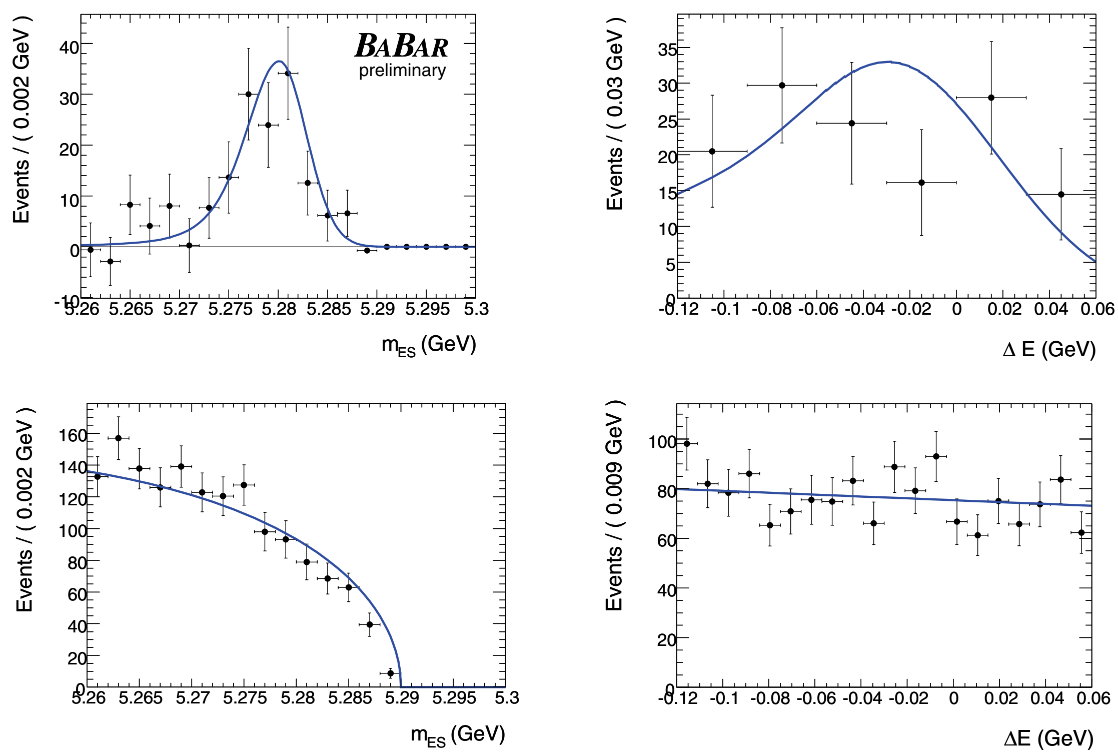

Figure 2: Distributions of kinematic variables (left) $m_{\rm ES}$ and (right) ΔE for the $K^+K^-K^0_S(\pi^0\pi^0)$ subsample: (top) signal, (bottom) continuum background. The points are data events weighted with the ${}_s\mathcal{P}lot$ technique [11], and the curves are the PDF shapes used in the ML fit (Sec. 3).

order to reduce background from π^0 decays, we reject an EMC K_L^0 candidate cluster if it forms an invariant mass between 100 and 150 MeV/c^2 with any other neutral cluster in the event under the $\gamma\gamma$ hypothesis, or if it has energy greater than 1 GeV and contains two shower maxima consistent with two photons from a π^0 decay. The remaining background of K_L^0 candidates due to photons and overlapping showers is further reduced with the use of a selector based on the *Boosted Decision Trees* algorithm [12, 13]. This selector is constructed from cluster shape variables, trained with Monte Carlo events, and tested on Initial State Radiation $e^+e^- \to \phi(\to K_S^0 K_L^0)\gamma$ events and reconstructed $B^0 \to J/\psi K_L^0$ candidates, which give a very pure sample of K_L^0 candidates.

We use the kinematic variable ΔE to characterize the signal and background. This variable, computed after the mass constraint on the B^0 candidate, has a resolution of about 3.0 MeV for EMC events, and about 4.0 MeV for IFR events. For signal events, ΔE is expected to peak at zero, with a broad tail for positive values of ΔE. We require $\Delta E < 30$ MeV, in order to be able to determine the shape of background under the signal peak. The mean value and the resolution of this variable has been taken from reconstructed $B^0 \to J/\psi K_L^0$ events.

In addition to the shape variables described in Sec. 2, we consider other variables, related to the missing energy in the event, to characterize events to the K_L^0 final state. The first, $p_{\rm miss}^T$, is the difference between the $\Upsilon(4S)$ energy and the total measured energy of the event, not including the K_L^0 candidate, projected onto the plane transverse to the beam axis. We also use the angle between $p_{\rm miss}^T$ and the reconstructed K_L^0 direction, and the difference between the total visible energy of the event and the two reconstructed kaon energies. The latter corresponds to the unmeasured K_L^0 energy, and has a somewhat different distribution in signal than in continuum background events. These three variables are used as inputs to a Fisher discriminant which has been trained on Monte Carlo samples and validated on data control samples.

We optimized the selections on all of these variables for maximum sensitivity in the measurement of *CP* parameters. The selection is optimized independently in the region $m_{K^+K^-} < 1.1$ GeV/c^2 and in the rest of the Dalitz plot, because the higher K^+K^- mass region gets more background from low momentum neutral candidates, for which the separation between photons and K_L^0 is worse. The final average efficiency of the selection is about 25% in the low-mass region and 10% for the rest of events.

The ΔE distribution, with the result of the fit superimposed, is shown in Fig. 3, after making a requirement on the ratio of signal likelihood to signal-plus-background likelihood to enhance the signal.

2.4 $B^+ \to \phi K^+$

We use the $B^+ \to \phi K^+$ decay to measure the charge asymmetry, the P-wave fraction, and the relative phase between the S and P waves in the $\phi(1020)$ region. The selection of the ϕ meson candidate is done by applying an invariant K^+K^- mass cut defined as $1.0045 < m_{K^+K^-} < 1.0345$ GeV/c^2. For the bachelor K^+ candidate from the B^+ decay the track requirements are the same as for the ϕ daughters but we apply a more restrictive kaon identification criterion.

The distributions of $m_{\rm ES}$ and $m_{K^+K^-}$ variables after a cut on the ratio of signal and background probabilities is shown in Figure 4.

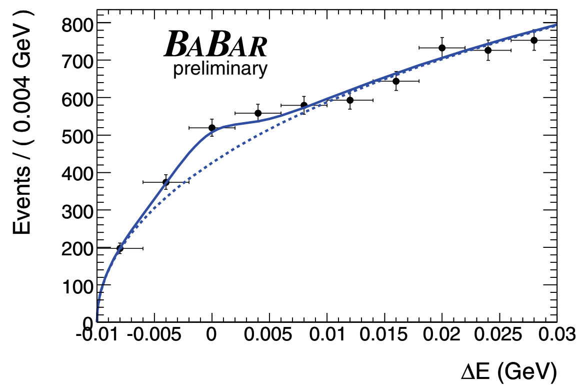

Figure 3: Distribution of the kinematic variable ΔE for the $K^+K^-K^0_L$ subsample. The solid line represents the total likelihood, while the dashed line represents the sum of continuum and $B\overline{B}$ background. A requirement on the ratio of signal likelihood to signal-plus-background likelihood is applied to enhance the signal, with an efficiency of about 30% for signal.

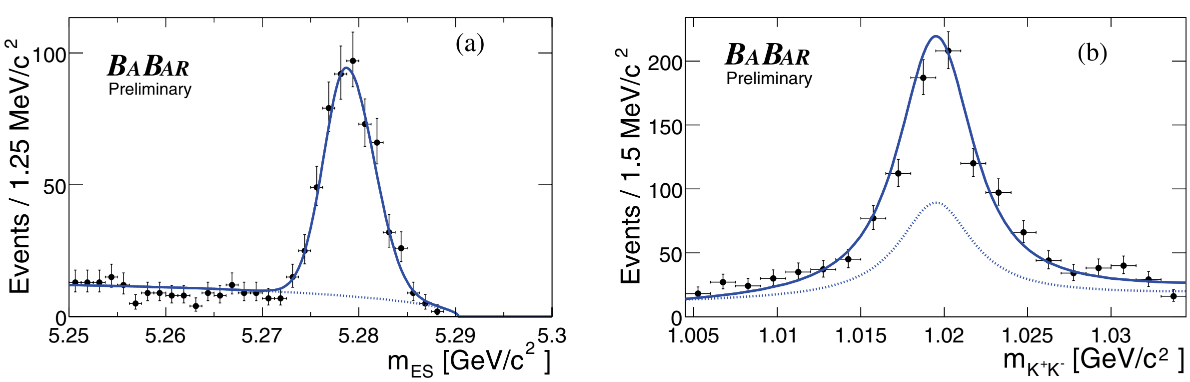

Figure 4: Distributions of the event variables (a) m_{ES} and (b) $m_{K^+K^-}$ in the ϕK^+ final state after reconstruction and a requirement on the likelihood calculated without the plotted variable. The efficiency for the selection and likelihood requirements is 78% for (a) and 95% for (b). The solid line represents the fit result for the total event yield and the dotted line for the background.

3 ANALYSIS OF THE DALITZ PLOT

We analyze selected events in all neutral B samples using a maximum likelihood fit with the likelihood function $\mathcal{L}$ for each subsample, defined as

$$\mathcal{L} = \exp\left(-\sum_i n_i\right) \prod_j \left[\sum_i n_i \mathcal{P}_{i,j}\right] \tag{1}$$

where j runs over all events in the sample, and n_i is the yield for event category i. The probability density function (PDF) $\mathcal{P}$ is formed from multiple observables as

$$\mathcal{P} \equiv \mathcal{P}(m_{\rm ES}) \cdot \mathcal{P}(\Delta E) \cdot \mathcal{P}_{DP}(m_{K^+K^-}, \cos\theta_H, \Delta t, q_{tag}) \otimes \mathcal{R}(\Delta t, \sigma_{\Delta t}). \tag{2}$$

Here $\cos\theta_H$ is the cosine of the helicity angle between the K^+ and the K^0 in the K^+K^- center-of-mass frame, q_{tag} is the flavor of the initial state, and $\Delta t = t_{rec} - t_{tag}$ is the difference of the proper decay times of the two B-mesons. $\sigma_{\Delta t}$ is the error on Δt. The PDF for the time-dependent Dalitz plot, $\mathcal{P}_{DP}$, is described in detail later in the text. $\mathcal{R}$ is a standard Δt resolution function with parameters evaluated in exclusive B^0 decays into final states with a charm meson as in our CP-asymmetry measurements in $J/\psi K^0_S$ decays [6]. For the $K^+K^-K^0_L$ submode, the $m_{\rm ES}$ variable does not enter the likelihood function defined in Eq. (2).

In all $K^+K^-K^0$ submodes, the signal components of the PDFs for $\mathcal{P}(m_{\rm ES})$ and $\mathcal{P}(\Delta E)$ are parameterized using modified Gaussian distributions: $\mathcal{P} = \exp[-(x-x_0)^2/(2\sigma^2_\pm + \alpha_\pm(x-x_0)^2)]$, where x is the dependent variable. We determine the parameters x_0, σ_+, σ_-, α_+, and α_- using simulated events, and fix them in fits to data. For $x < x_0$ ($x > x_0$), the parameters σ_-, α_- (σ_+, α_+) are used. In the $B^+ \to \phi K^+$ mode, the signal $m_{\rm ES}$ distribution is parameterized as above, but with $\alpha_\pm$ set to zero. The signal ΔE distribution is parameterized as the sum of two Gaussian distributions.

In all applicable submodes, we use the Argus function to model the continuum background component of $\mathcal{P}(m_{\rm ES})$ [14]. For $\mathcal{P}(\Delta E)$, linear shapes are used for the continuum background, except for the $K^+K^-K^0_L$ submode. In that case, we use a reflection of the Argus function.

In the $K^+K^-K^0_S(\pi^0\pi^0)$ and $K^+K^-K^0_L$ submodes, $B\overline{B}$ background components are parameterized with the same functional forms as the continuum backgrounds. Due to non-negligible correlation between $m_{\rm ES}$ and ΔE for $B\overline{B}$ background in the $K^+K^-K^0_S(\pi^0\pi^0)$ submode, we construct that PDF component as a two-dimensional histogram PDF in those variables.

3.1 Background Decays in the Time-Dependent Dalitz Plot

The Dalitz plot for the continuum background is parameterized using a two-dimensional histogram PDF in the variables $m_{K^+K^-}$ and $\cos\theta_H$. The histogram is filled with candidates from the region $5.2 < m_{\rm ES} < 5.26$ GeV/c^2 for the $K^+K^-K^0_S$ submodes. For the $K^+K^-K^0_L$ submode, candidates from the region $20 < \Delta E < 40$ MeV are used. The Δt distribution is described with a separate PDF which, similarly to our previous measurement [9], uses a double-Gaussian resolution function and allows a fraction of decays to have a non-zero lifetime. For the $B^+ \to \phi K^+$ mode, the continuum background distribution in $m_{K^+K^-}$ is modeled with the sum of a relativistic Breit-Wigner function (see Section 3.2) and a second-order polynomial.

We estimate the amount of $B\overline{B}$ background from Monte Carlo events and again describe the Dalitz plot using a two-dimensional histogram PDF. The $B\overline{B}$ background in $K^+K^-K^0_S$ modes is almost purely combinatorial and is a few percent of the total background. The $K^+K^-K^0_L$

sample, in addition to combinatorial $B\overline{B}$ background, contains decays into 4-body final states where a pion is missed in the reconstruction (Sec. 2.3). Such decays (e.g. $K^+K^-K^*$) are simulated with the assumption that the phase space contains the same distribution in the Dalitz plot as in $B^+ \to K^+K^+K^-$ and $B^0 \to K^+K^-K^0_S$ decays: ϕK^*, a wide scalar at 1.5 GeV/c^2 and a non-flat non-resonant distribution. The Δt distribution is described as a separate PDF that has a non-zero lifetime. The time-dependent *CP* asymmetry of this PDF, set to zero in the reference fit, is varied as a systematic uncertainty.

The decays $B^0 \to D^+K^-$ ($D^+ \to K^+K^0$) and $B^0 \to D_s^+K^-$ ($D_s^+ \to K^+K^0$) are kinematically indistinguishable from signal decays. We include non-interfering amplitudes for these modes in our Dalitz plot model, parameterizing the $D_{(s)}$ mesons on the Dalitz plot as Gaussian distributions with widths taken from studies of simulated events.

3.2 Signal Decays in the Time-Dependent Dalitz Plot

When the flavor of the initial state q_{tag}, and the difference of the proper decay times Δt, are measured, the time- and flavor-dependent decay rate over the Dalitz plot can be written as

$$d\Gamma = \frac{1}{(2\pi)^3}\frac{1}{32M^3_{B^0}}\frac{e^{-|\Delta t|/\tau_{B^0}}}{4\tau_{B^0}} \times \Big[\, |\mathcal{A}|^2 + |\bar{\mathcal{A}}|^2 \pm q_{tag}\ 2Im\,(\bar{\mathcal{A}}\mathcal{A}^*)\sin\Delta m_d\Delta t - q_{tag}\left(|\mathcal{A}|^2 - |\bar{\mathcal{A}}|^2\right)\cos\Delta m_d \Delta t \, \Big], \tag{3}$$

where plus (minus) sign is for decays to $K^+K^-K^0_S$ ($K^+K^-K^0_L$) and $q_{tag} = +1$ (-1) when the other B meson is identified as a B^0 ($\overline{B}^0$) using a neural network technique [6]. Approximately 75% of the signal events have tagging information and contribute to the measurement of CP violation parameters. After accounting for the mistag rate, the effective tagging efficiency is $(30.4 \pm 0.3)\%$. Events without tagging information are still included in the fit as they contribute to the determination of the Dalitz plot parameters. Decay amplitudes $\mathcal{A}$ and $\bar{\mathcal{A}}$ are defined in (5) and (6) below. M_{B^0}, τ_{B^0}, and Δm_d are the mass, lifetime, and mixing frequency of the B^0 meson, respectively [2].

Four-momentum conservation in a three-body decay gives the relation $M^2_{B^0} + m_1^2 + m_2^2 + m_3^2 = m^2_{12} + m^2_{13} + m^2_{23}$, where $m^2_{ij} = (p_i + p_j)^2$ is the square of the invariant mass of a daughter pair. This constraint leaves a choice of two independent Dalitz plot variables to describe the decay dynamics of a spin-zero particle. In this analysis we choose the K^+K^- invariant mass $m_{K^+K^-}$ and the cosine of the helicity angle $\cos\theta_H$. The PDF for the Dalitz plot rate becomes

$$\mathcal{P}_{DP} \propto d\Gamma(m_{K^+K^-}, \cos\theta_H, \Delta t, q_{tag}) \cdot \varepsilon(m_{K^+K^-}, \cos\theta_H) \cdot |J| \otimes \mathcal{R}(\Delta t, \sigma_{\Delta t}), \tag{4}$$

where the Jacobian $|J(m_{K^+K^-})| = (2m_{K^+K^-})(2qp)$ is given in terms of the charged kaon momentum q and neutral kaon momentum p, in the K^+K^- frame. The efficiency ε is calculated from high-statistics samples of simulated events and depends on the position on the Dalitz plot.

The amplitude $\mathcal{A}$ ($\bar{\mathcal{A}}$) for the decay $B^0 \to K^+K^-K^0$ ($\overline{B}^0 \to K^-K^+\overline{K}^0$) is, in our isobar model, written as a sum of decays through intermediate resonances:

$$\mathcal{A} = \sum_r c_r(1+b_r)e^{i(\phi_r+\delta_r+\beta)} \cdot f_r, \qquad \text{and} \tag{5}$$

$$\bar{\mathcal{A}} = \sum_r c_r(1-b_r)e^{i(\phi_r-\delta_r-\beta)} \cdot \bar{f}_r. \tag{6}$$

The parameters c_r and ϕ_r are the magnitude and phase of the amplitude of component r, and we allow for different isobar coefficients for B^0 and $\overline{B}^0$ decays through the asymmetry parameters

b_r and δ_r. The parameter β is the CKM angle β, coming from B^0-$\overline{B}^0$ mixing. The function $f_r = F_r \times T_r \times Z_r$ describes the dynamic properties of a resonance r, where F_r is the form-factor for the resonance decay vertex, T_r is the resonant mass-lineshape, and Z_r describes the angular distribution in the decay [15, 16].

Our model includes the $\phi(1020)$, where we use the Blatt-Weisskopf centrifugal barrier factor $F_r = 1/\sqrt{1+(Rq)^2}$ [15], where q is the daughter momentum in the resonance frame, and R is the effective meson radius, taken to be $R = 1.5$ GeV (0.3 fm). For the scalar decays included in our model ($f_0(980)$, $X_0(1550)$, and χ_{c0}), we use a constant form-factor. Note that we have omitted a similar centrifugal factor for the B^0 decay vertex into the ϕK^0 intermediate state since its effect is negligible due to the small width of the $\phi(1020)$ resonance.

The angular distribution is constant for scalar decays, whereas for vector decays $Z = -4\vec{q}\cdot\vec{p}$, where $\vec{q}$ is the momentum of the resonant daughter, and $\vec{p}$ is the momentum of the third particle in the resonance frame. We describe the line-shape for the $\phi(1020)$, $X_0(1550)$, and χ_{c0} using the relativistic Breit-Wigner function

$$T(m) = \frac{1}{m_r^2 - m_{K^+K^-}^2 - im_r\Gamma(m)}, \tag{7}$$

where m_r is the resonance pole mass. The mass-dependent width is given as $\Gamma(m_{K^+K^-}) = \Gamma_r\,(q/q_r)^{2L+1}\,(m_r/m_{K^+K^-})\,(F_r(q)/F_r(q_r))^2$, where L is the resonance spin and $q = q_r$ when $m_{K^+K^-} = m_r$. For the $\phi(1020)$ and χ_{c0} parameters, we use average measurements [2]. The $X_0(1550)$ is less well-established. Previous Dalitz plot analyses of $B^+ \to K^+K^+K^-$ [17, 18] and $B^0 \to K^+K^-K^0$ decays [19] report observations of a scalar resonance at around 1.5 GeV/c^2. The scalar nature has been confirmed by partial-wave analyses [9, 18]. However, previous measurements report inconsistent resonant widths: 0.145 ± 0.029 GeV/c^2 [17] and 0.257 ± 0.033 GeV/c^2 [18]. Branching fractions also disagree, so the nature of this component is still unclear [20]. In our reference fit, we take the resonance parameters from Ref. [18], which is based on a larger sample of $B\overline{B}$ decays than Ref. [17], and consider the narrower width given in the latter in the systematic error studies.

The $f_0(980)$ resonance is described with the coupled-channel (Flatté) function

$$T(m_{K^+K^-}) = \frac{1}{m_r^2 - m_{K^+K^-}^2 - im_r(\rho_K g_K + \rho_\pi g_\pi)}, \tag{8}$$

where $\rho_K(m_{K^+K^-}) = 2\sqrt{1-4m_K^2/m_{K^+K^-}^2}$, $\rho_\pi(m_{K^+K^-}) = 2\sqrt{1-4m_\pi^2/m_{K^+K^-}^2}$, and the coupling strengths for the KK and $\pi\pi$ channels are taken as $g_\pi = 0.165 \pm 0.018$ GeV/c^2, $g_K/g_\pi = 4.21 \pm 0.33$, and $m_r = 0.965 \pm 0.010$ GeV/c^2 [21].

In addition to resonant decays, we include non-resonant amplitudes. Existing models consider contributions from contact terms or higher-resonance tails [22, 23, 5], but they do not capture features observed in data. We rely on a phenomenological parameterization [17] and describe the non-resonant terms as

$$\mathcal{A}_{NR} = \left(c_{12}e^{i\phi_{12}}e^{-\alpha m_{12}^2} + c_{13}e^{i\phi_{13}}e^{-\alpha m_{13}^2} + c_{23}e^{i\phi_{23}}e^{-\alpha m_{23}^2}\right)\cdot(1+b_{NR})\cdot e^{i(\beta+\delta_{NR})} \tag{9}$$

and similarly for $\bar{\mathcal{A}}_{NR}$. The slope of the exponential function is consistent among previous measurements in both neutral and charged B decays into three kaons [17, 18, 19], and we use $\alpha = 0.14 \pm 0.02$ GeV$^{-2}\cdot c^4$.

We compute the direct CP-asymmetry parameters for resonance r from the asymmetries in amplitudes (b_r) and phases (δ_r) given in Eqs. (5, 6). We define the rate asymmetry as

$$A_{CP}(r) = \frac{|\bar{\mathcal{A}}_r|^2 - |\mathcal{A}_r|^2}{|\bar{\mathcal{A}}_r|^2 + |\mathcal{A}_r|^2} = \frac{-2b_r}{1+b_r^2}, \tag{10}$$

and $\beta_{\mathit{eff}}(r) = \beta + \delta_r$ is defined as the total phase asymmetry. The fraction for resonance r is computed

$$\mathcal{F}_r \;=\; \frac{\int d\cos\theta_H \; dm_{K^+K^-} \cdot |J| \cdot (|\mathcal{A}_r|^2 + |\bar{\mathcal{A}}_r|^2)}{\int d\cos\theta_H \; dm_{K^+K^-} \cdot |J| \cdot (|\mathcal{A}|^2 + |\bar{\mathcal{A}}|^2)}. \tag{11}$$

The sum of the fractions can differ from unity due to interference between the isobars.

3.3 Calculation of Angular Moments

As an alternative description that is less dependent on a resonance model, we analyze the Dalitz plot in terms of moments of the cosine of the helicity angle, $\cos\theta_H$, in $B^+ \to \phi K^+$ and $B^0 \to K^+K^-K^0_S(\pi^+\pi^-)$ decays. We only assume that the total amplitude is the sum of the two lowest partial waves, and ignore direct CP-violation effects:

$$\mathcal{A}\;(\bar{\mathcal{A}}) \;=\; A_s P_0(\cos\theta_H) \;\pm\; e^{i\phi} A_p P_1(\cos\theta_H), \tag{12}$$

where $\phi = \phi_P - \phi_S$ is the relative phase between S and P-wave strengths. The $\pm$ sign corresponds to B^0 or $\overline{B}^0$ decays, respectively. P_0 and P_1 are Legendre polynomials that describe the amplitude dependence on $\cos\theta_H$ for S-wave and P-wave decays, respectively. Integrating Eq. (4) over Δt, the tag-dependent decay rate can be written in terms of Legendre polynomials as follows:

$$\frac{d\Gamma}{d\cos\theta_H \cdot dm_{K^+K^-} \cdot |J|} \;=\; \sum_{l=0,1,2} \langle P_l \rangle \times P_l(\cos\theta_H) \tag{13}$$

$$= \frac{A_s^2 + A_p^2}{\sqrt{2}} \times P_0(\cos\theta_H) \;+\; \sqrt{\frac{2}{5}} A_p^2 \times P_2(\cos\theta_H) - \frac{q_{tag}\cdot\langle D\rangle}{(\Delta m_d \tau_{B^0})^2 + 1} \times \frac{2A_sA_p}{\sqrt{2}} \cos\phi \times P_1(\cos\theta_H), \tag{14}$$

where the flavor tagging is necessary to measure the S-P wave interference term proportional to P_1. In the decay $B^0 \to K^+K^-K^0$, this term is diluted by the imperfect tagging $\langle D\rangle$ and the $B^0 - \overline{B}^0$ mixing. In charged B decays to the $K^+K^+K^-$ final state we set $\Delta m_d = 0$ and $\langle D\rangle = 1$ since q_{tag} corresponds to the charge of the final state. Using our data sample, we compute the Legendre moments $\langle P_l\rangle$,

$$\langle P_l \rangle \;\approx\; \sum_i P_l(\cos\theta_H, i)\; \mathcal{W}(i)/\varepsilon(i), \tag{15}$$

where $\mathcal{W}$ is the weight for event i to belong to the signal sample [11]. These weights are computed from maximum likelihood fits that do not use the mass or the helicity angle in the fit. Finally, the fraction of P-wave decays is computed as $f_p = \sqrt{5/4} \cdot \langle P_2\rangle \,/\, \langle P_0\rangle$ [9].

4 RESULTS

4.1 Dalitz Plot and Angular Moments

In order to determine parameters of the Dalitz plot model, we perform a fit to 3091 $B^0 \to K^+K^-K^0_S(\pi^+\pi^-)$ candidates in the full Dalitz plot. In this step we assume that all decays have the same *CP*-asymmetry parameters. We vary the event yields, isobar coefficients of the Dalitz plot model, and two *CP*-asymmetry parameters averaged over the Dalitz plot. We find a signal yield of 879 ± 36 events. The isobar amplitudes, phases, and fractions are listed in Table 1. The sum of resonant fractions in our DP model is different from 100% due to interference between resonances.

We compare our fractions with other Dalitz plot analyses using flavor symmetry [24]. We find consistent fractions for decays through the $\phi(1020)$ resonances with the $B^+ \to K^+K^+K^-$ decay [17, 18]. The fraction of $f_0(980)K^0$ decays is consistent with our $B^+ \to K^+K^+K^-$ analysis, and all $B^+ \to K^+\pi^+\pi^-$ Dalitz plot analyses [17, 18, 25]. The fraction of non-resonant decays, which is predicted to be half of the contribution in $B^+ \to K^+K^+K^-$ [24], is harder to compare since existing measurements in the charged mode are inconsistent. Our result agrees well with *BABAR*'s result [18], and is within two standard deviations of Belle's result [17]. Determination of the wide scalar resonance at 1.5 GeV/c^2, labeled as $X_0(1550)$, is even more uncertain. Using the same resonant parameters we find a much smaller fraction than in *BABAR*'s analysis [18], but our solution is more consistent with Belle's $B^+ \to K^+K^+K^-$ analysis [17].

In order to achieve better statistical precision in measurements of *CP*-asymmetry parameters that are described in the following sections, we combine the $K^+K^-K^0_S(\pi^+\pi^-)$ sample with samples of 1599 $B^0 \to K^+K^-K^0_S(\pi^0\pi^0)$ and 22341 $B^0 \to K^+K^-K^0_L$ candidates. Fixing the coefficients of the isobar model to the values extracted from the $K^+K^-K^0_S(\pi^+\pi^-)$ submode, we find signal yields of 138 ± 17 and 499 ± 52 events in the $K^+K^-K^0_S(\pi^0\pi^0)$ and $K^+K^-K^0_L$ submodes, respectively. Projection plots for the Dalitz plot variables are shown for all three submodes in Figure 5.

Decay	Amplitude c_r	Phase ϕ_r	Fraction $\mathcal{F}_r$ (%)
$\phi(1020)K^0$	0.0098 ± 0.0016	-0.11 ± 0.31	12.9 ± 1.3
$f_0(980)K^0$	0.528 ± 0.063	-0.33 ± 0.26	22.3 ± 8.9
$X_0(1550)K^0$	0.130 ± 0.025	-0.54 ± 0.24	4.1 ± 1.8
NR (K^+K^-)	1 (fixed)	0 (fixed)	
(K^+K^0)	0.38 ± 0.11	2.01 ± 0.28	91 ± 19
(K^-K^0)	0.38 ± 0.16	-1.19 ± 0.37	
$\chi_{c0}K^0$	0.0343 ± 0.0067	1.29 ± 0.41	2.84 ± 0.77
D^+K^-	1.18 ± 0.24	–	3.18 ± 0.89
$D_s^+K^-$	0.85 ± 0.20	–	1.72 ± 0.65

Table 1: Isobar amplitudes, phases, and fractions from the fit to the $B^0 \to K^+K^-K^0_S(\pi^+\pi^-)$ sample. Three rows for non-resonant contribution correspond to coefficients of exponential functions in Eq. (9), while the fraction is given for the combined amplitude. Errors are statistical only.

As an additional crosscheck of our Dalitz plot model, we compute angular moments and extract strengths of the partial waves in K^+K^- mass bins using the $B^+ \to \phi K^+$ and $B^0 \to K^+K^-K^0_S(\pi^+\pi^-)$ samples. In this approach we rely only on the assumption that the two lowest partial waves are present, but make no other assumption on the decay model. We confirmed the non-existence of higher partial waves by determining that higher angular moments ($\langle P_{3-5}\rangle$) are

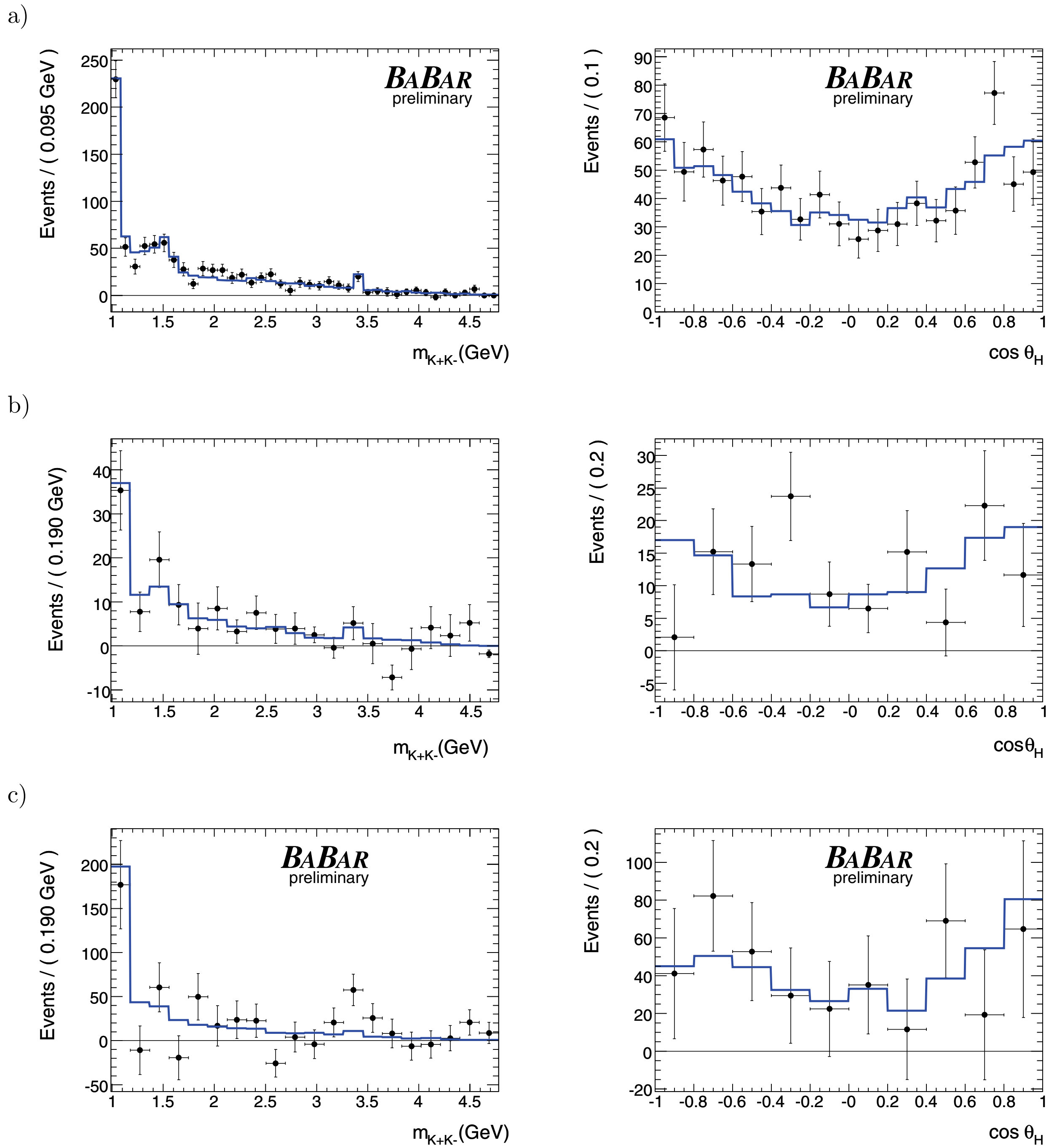

Figure 5: Distributions of the Dalitz plot variables (left) $m_{K^+K^-}$ and (right) $\cos\theta_H$ for signal events (points) compared with the fit PDF in the following sub-samples: a) $K^+K^-K^0_S(\pi^+\pi^-)$, b) $K^+K^-K^0_S(\pi^0\pi^0)$, c) $K^+K^-K^0_L$. All sub-samples use the same Dalitz plot model but have different efficiencies so the resulting distributions differ.

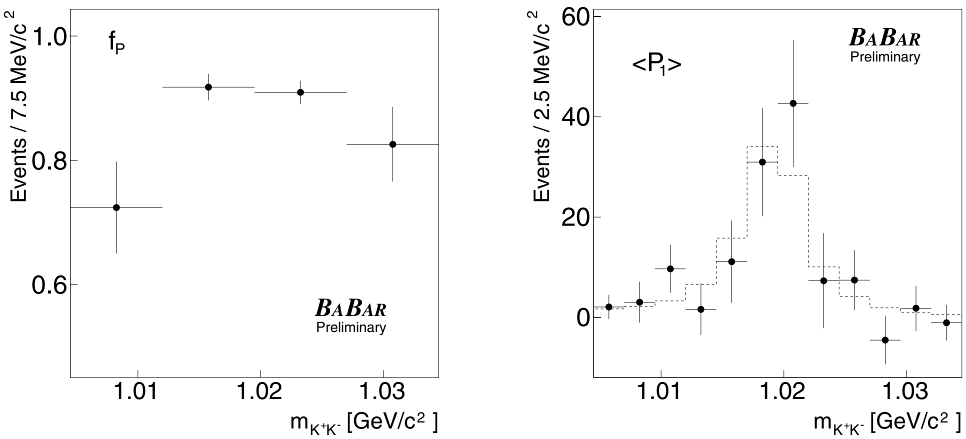

Figure 6: ϕK^+: (left) The relative P-wave fraction f_p in the interval $1.0045 < m_{K^+K^-} < 1.0345$ GeV/c^2. (right) The moment $\langle P_1 \rangle$ calculated with the $\phi(1020)$ helicity angle defined with respect to the kaon of the same charge as the B meson. The dashed line corresponds to the fit result.

consistent with zero.

From the fit to 4947 $B^+ \to \phi K^+$ candidates, we find 624 ± 30 signal candidates in the mass region $1.0045 < m_{K^+K^-} < 1.0345$ GeV/c^2. The event weights $\mathcal{W}_i$ are computed from the likelihood without $m_{K^+K^-}$ and $\cos\theta_H$. From $\langle P_0 \rangle$ and $\langle P_2 \rangle$ we obtain the average fraction $f_p = 0.891 \pm 0.014$. The distribution of f_p in four bins of $m_{K^+K^-}$ is shown in Fig. 6. In order to determine the relative phase between S- and P-waves, we make a χ^2 minimization of the moment $\langle P_1 \rangle$ given with Eq. (14), by varying the phase while keeping S- and P-wave strengths fixed. For the S-wave we assume negligible energy dependence in the $\phi(1020)$ region and parameterize the resonance shape with a relativistic Breit-Wigner function. We estimate a phase difference between P- and S-wave of $(78 \pm 20)^\circ$; the systematic error due to the choice of the S-wave model and the χ^2 scan method is negligible. The moment $\langle P_1 \rangle$ from data, with the best phase solution superimposed, is displayed in the right-hand plot of Figure 6.

Similarly, we compute the P-wave strength as a function of K^+K^- invariant mass in $B^0 \to K^+K^-K^0_S(\pi^+\pi^-)$ decays as shown in Figure 7. We find the total fraction of P-wave in our sample is 0.29 ± 0.03 (stat) integrated over the entire Dalitz plot, which is consistent with our previous measurement [9]. In our model, this P-wave contribution originates from $\phi(1020)K^0_S$ decays, and non-resonant events with $K^+K^0_S$ and $K^-K^0_S$ mass dependence that reflects into an effective P-wave that enhances the central part of the plot in Figure 7.

4.2 *CP* Asymmetry in the Low-K^+K^- Mass Region

In order to measure *CP*-asymmetry parameters for components with low-K^+K^- mass with reduced model-dependence from the rest of the Dalitz plot, we select events using a cut of $m_{K^+K^-} < 1.1$ GeV/c^2. After this selection, there are 836 $K^+K^-K^0_S(\pi^+\pi^-)$ candidates, 202 $K^+K^-K^0_S(\pi^0\pi^0)$ candidates, and 4923 $K^+K^-K^0_L$ candidates remaining. The most significant contribution in this region comes from $\phi(1020)K^0$ and $f_0(980)K^0$ decays, with a smaller contribution from a low-K^+K^- tail of non-resonant decays. We vary the isobar parameters for the $\phi(1020)$ and fix all other

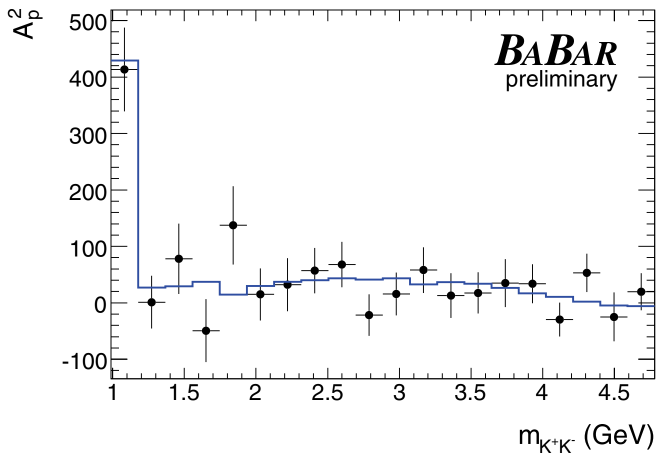

Figure 7: $K^+K^-K^0_S(\pi^+\pi^-)$: The absolute strength of P-wave decays as a function of K^+K^- mass. The points are signal-weighted data and the histogram corresponds to the Dalitz plot model.

components to the results of the full Dalitz plot fit. We also vary the *CP* amplitude and phase asymmetries for the $\phi(1020)$ and $f_0(980)$. The asymmetry for the other components is fixed to the SM expectation. We perform a fit to the $K^+K^-K^0_S(\pi^+\pi^-)$ submode, then perform an additional fit to the entire $K^+K^-K^0$ sample. We find signal yields of 252 ± 19, 35 ± 9, and 195 ± 33 events for $K^+K^-K^0_S(\pi^+\pi^-)$, $K^+K^-K^0_S(\pi^0\pi^0)$, and $K^+K^-K^0_L$ respectively. Fig. 8 shows projections of the Dalitz plot distributions of events in this region. The *CP*-asymmetry results are listed in Table 2; the systematic uncertainties will be described in Sec. 5. The left plots in Fig. 9 show distributions of Δt for B^0-tagged and $\overline{B}^0$-tagged events, and the asymmetry $\mathcal{A}(\Delta t) = (N_{B^0} - N_{\overline{B}^0})/(N_{B^0} + N_{\overline{B}^0})$, obtained with the ${}_s\mathcal{P}lot$ event-weighting technique [11]. Correlation coefficients r between *CP* parameters, found in the fit to the combined sample, are also shown in Table 2.

Name	Fitted Value		Correlation (Combined)			
	$K^+K^-K^0_S$ $(\pi^+\pi^-)$	Combined	1	2	3	4
1 $A_{CP}(\phi K^0)$	-0.10 ± 0.23	$-0.18 \pm 0.20 \pm 0.10$	1.0	-0.08	-0.27	0.11
2 $\beta_{eff}(\phi K^0)$	0.02 ± 0.16	$0.06 \pm 0.16 \pm 0.05$		1.0	0.46	0.74
3 $A_{CP}(f_0 K^0)$	0.36 ± 0.33	$0.45 \pm 0.28 \pm 0.10$			1.0	0.20
4 $\beta_{eff}(f_0 K^0)$	0.04 ± 0.18	$0.18 \pm 0.19 \pm 0.04$				1.0

Table 2: *CP*-violation parameters for $B^0 \to K^+K^-K^0$ for $m_{K^+K^-} < 1.1$ GeV/c^2. For the combined $K^+K^-K^0$ sample, the first error is statistical and the second is systematic. For the $K^+K^-K^0_S$ submode, only statistical errors are shown.

The decay $B^0 \to \phi K^0$, with highly suppressed tree amplitudes, is, in terms of theoretical uncertainty, the cleanest channel to interpret possible deviations of the *CP*-violation parameters from the SM expectations. Values of β_{eff} are consistent with the value found in $[c\bar{c}]K^0$ decays [6, 7].

As a consistency check we compare $\beta_{eff}(\phi K^0)$ against a quasi-two-body approach (Q2B) that selects events around the ϕ resonance, $1.0045 < m_{K^+K^-} < 1.0345$ GeV/c^2, in order to increase the purity of P-wave decays. We add separate $\cos\theta_H$ and $m_{K^+K^-}$ PDFs to the likelihood to

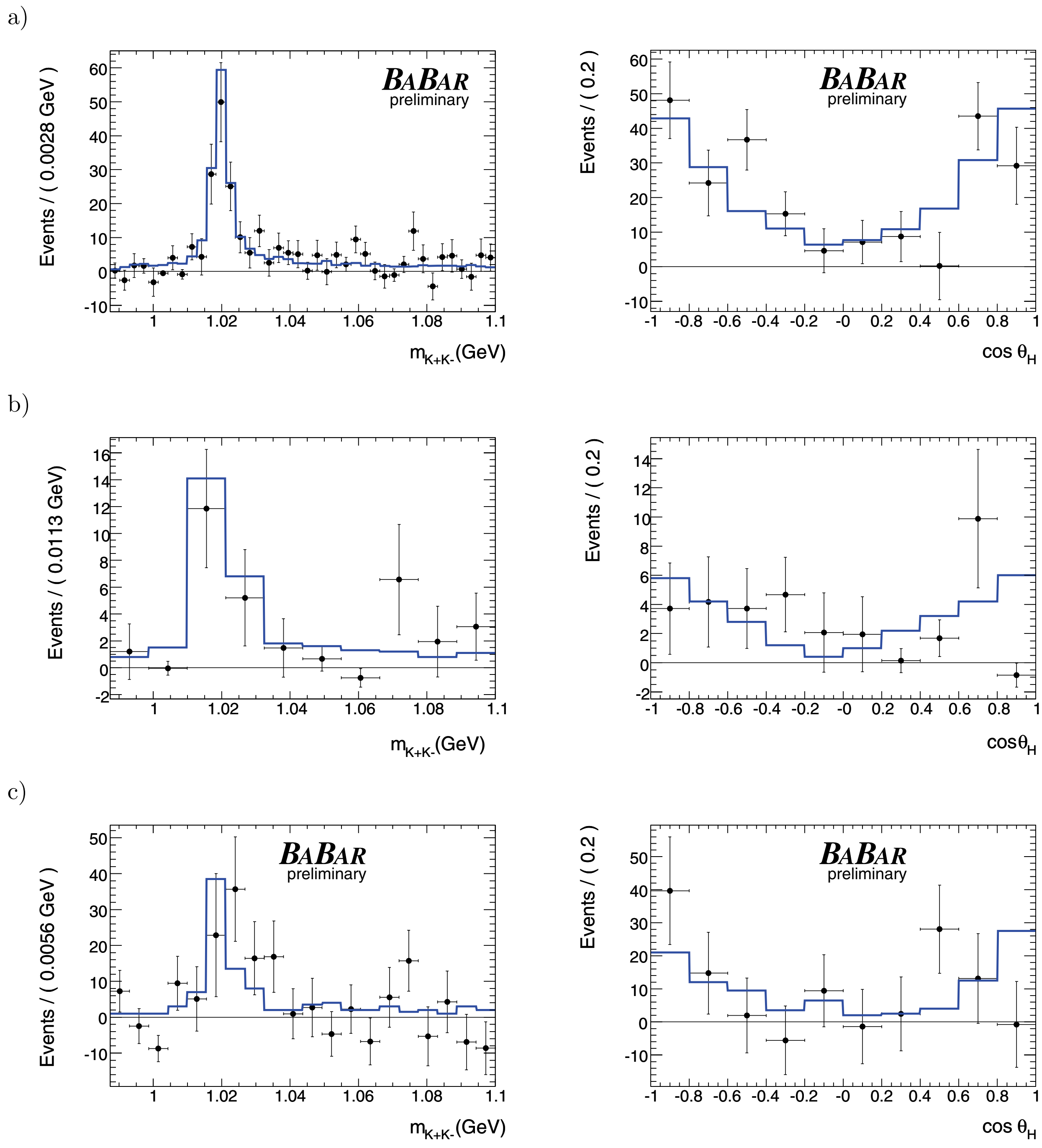

Figure 8: For the low-K^+K^- mass Dalitz plot fit, distributions of the Dalitz plot variables (left) $m_{K^+K^-}$ and (right) $\cos\theta_H$ for signal events (points) compared with the fit PDF in the following sub-samples: a) $K^+K^-K^0_S(\pi^+\pi^-)$, b) $K^+K^-K^0_S(\pi^0\pi^0)$, c) $K^+K^-K^0_L$.

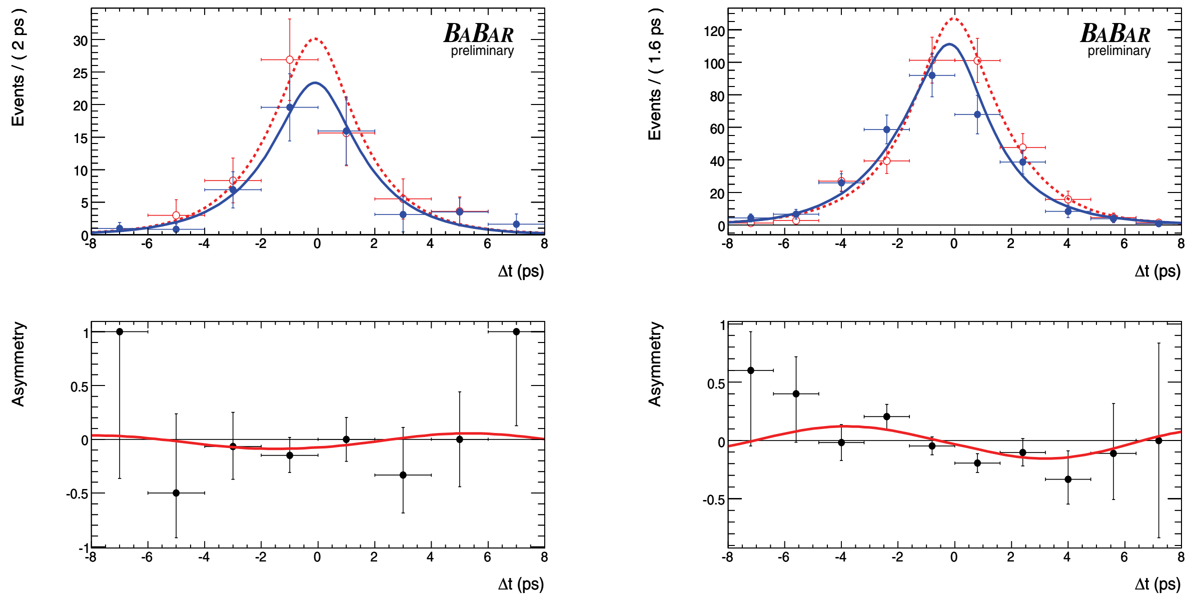

Figure 9: (top) Δt distributions and (bottom) asymmetries in the $K^+K^-K^0_S(\pi^+\pi^-)$ submode for (left) $1.0045 < m_{K^+K^-} < 1.0345$ GeV/c^2 and (right) the whole Dalitz plot. For the Δt distributions, B^0- ($\overline{B}^0$-) tagged signal-weighted events are shown as filled (open) circles, with the PDF projection in solid blue (dashed red).

further suppress the S-wave decays. From this fit we find 166 ± 15 ϕK^0_S and 151 ± 22 ϕK^0_L signal events. The CP parameters in the channel $B^0 \to \phi K^0_S$ only are: $S_{\phi K} = 0.10 \pm 0.29$ and $C_{\phi K} = 0.28 \pm 0.20$; in the channel $B^0 \to \phi K^0_L$: $S_{\phi K} = 0.69 \pm 0.35$ and $C_{\phi K} = -0.28 \pm 0.33$, with statistical errors only. The simultaneous quasi-two-body fit to both ϕK^0 and flavor decay modes yields the result $S_{\phi K} = 0.39 \pm 0.23$ and $C_{\phi K} = 0.10 \pm 0.18$ which is fully consistent with the Dalitz plot result. In this comparison we neglect interference effects and use the approximation $S_{\phi K} \approx \sin(2\beta_{\mathit{eff}})(1-b^2)/(1+b^2)$ and $C_{\phi K} \approx -A_{CP}$ to relate the Dalitz plot CP-violation parameters to the Q2B CP-violation parameters for the ϕK^0 decay.

We also measure the direct CP asymmetry in $B^+ \to \phi K^+$ decays, defined as $A_{CP} = (N_{B^-} - N_{B^+})/(N_{B^-} + N_{B^+})$. In a fit for the ϕK^+ and ϕK^- yields we find $\mathcal{A}_{CP} = 0.046 \pm 0.046 \pm 0.017$.

4.3 Average *CP* Asymmetry in $B^0 \to K^+K^-K^0$

We fit the average CP-violation parameters β_{eff}, A_{CP} across the $B^0 \to K^+K^-K^0$ Dalitz plot, and remove an ambiguity in the solution for the mixing angle $\beta_{\mathit{eff}} \to \pi/2 - \beta_{\mathit{eff}}$, present in previous measurements of $\sin(2\beta_{\mathit{eff}})$ in penguin decays. In our analysis the reflection is removed due to interference between CP-even and CP-odd decays that give rise to a $\cos(2\beta_{\mathit{eff}})$ term, in addition to the $\sin(2\beta_{\mathit{eff}})$ terms that come from the interference of decays with and without mixing. Fit results for CP parameters are listed in Table 3 for both the $K^+K^-K^0_S(\pi^+\pi^-)$ submode and the entire sample. Δt projection plots for signal-weighted events [11], shown in the right plots of Fig. 9, clearly show a large phase difference between B^0 and $\overline{B}^0$ decays. The correlation coefficients r between the CP parameters are given in Table 3. The global correlation coefficients in the fit to the combined sample are 0.02 and 0.08 for β_{eff} and A_{CP}, respectively.

Name	Fitted Value	
	$K^+K^-K^0_S(\pi^+\pi^-)$	Combined
A_{CP}	-0.100 ± 0.089	$-0.034 \pm 0.079 \pm 0.025$
β_{eff}	0.354 ± 0.083	$0.361 \pm 0.079 \pm 0.037$
r	0.003	0.013

Table 3: Average *CP*-asymmetry parameters for the $B^0 \to K^+K^-K^0$ Dalitz plot. For the combined $K^+K^-K^0$ sample, the first error is statistical and the second is systematic. For the $K^+K^-K^0_S$ submode, only statistical errors are shown.

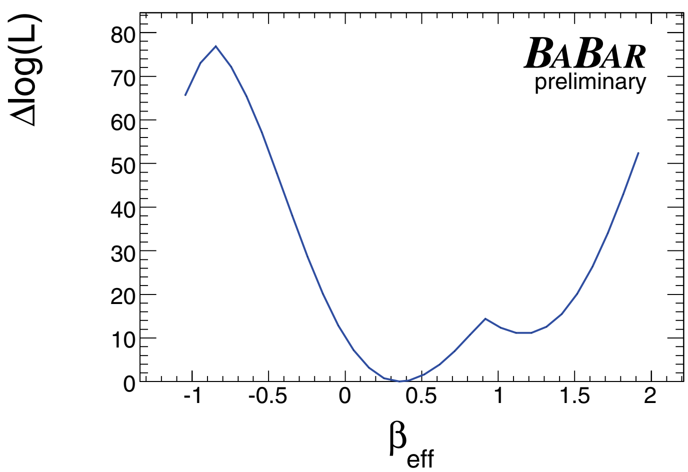

Figure 10: $K^+K^-K^0_S(\pi^+\pi^-)$: Change in the $\Delta\log(\mathcal{L})$ value as a function of β_{eff}.

Using the $K^+K^-K^0_S(\pi^+\pi^-)$ subsample, we estimate the significance of the nominal result for β_{eff} compared to the trigonometric reflection where $\beta_{\mathit{eff}} \to \pi/2 - \beta_{\mathit{eff}}$. In a collection of fits with both isobar coefficients and *CP*-asymmetry parameters allowed to vary, we randomize the initial parameter values and evaluate the likelihood separation between these two solutions. We find $\Delta\log(\mathcal{L}) = 10.4$, which excludes the reflection at a significance of 4.6 standard deviations. Note that a reflection $\beta_{\mathit{eff}} \to \beta_{\mathit{eff}} + \pi$ still remains since we measure the total phase difference between B^0 and $\overline{B}^0$ decays ($2\beta_{\mathit{eff}}$). A scan of the change in likelihood as a function of β_{eff} is shown in Figure 10.

5 SYSTEMATIC STUDIES

We study systematic effects on the *CP*-asymmetry parameters due to fixed parameters in the event-selection (m_{ES} and ΔE) PDFs. We assign systematic errors by comparing the fit with nominal parameters and with parameters smeared by their error, and assign the average difference as the systematic error. We account for a potential fit bias using values observed in studies with MC samples generated with the nominal Dalitz plot model. We take the largest values of the bias observed in these studies as the systematic error. We account for fixed Δt resolution parameters, B^0 lifetime, B^0-$\overline{B}^0$ mixing and flavor tagging parameters. We also assign an error due to interference between the CKM-suppressed $\bar{b} \to \bar{u}c\bar{d}$ and the favored $b \to c\bar{u}d$ amplitude for some tag-side B

decays [26]. Smaller errors due to beam-spot position uncertainty, detector alignment, and the boost correction are based on studies done in charmonium decays. In all fits we assume no direct CP violation in decays dominated by the $b \to c$ transition ($\chi_{c0}K^0$, $D_{(s)}K$).

Parameter	ϕK^0		$f_0 K^0$		$K^+K^-K^0$	
	A_{CP}	β_{eff}	A_{CP}	β_{eff}	A_{CP}	β_{eff}
Event selection	0.00	0.01	0.00	0.00	0.003	0.002
Fit Bias	0.04	0.01	0.04	0.02	0.004	0.010
Δt, vertexing	0.02	0.03	0.01	0.01	0.010	0.010
Tagging	0.01	0.00	0.01	0.00	0.021	0.002
Dalitz model	0.09	0.03	0.09	0.03	0.011	0.035
Total	0.10	0.05	0.10	0.04	0.025	0.037

Table 4: Summary of systematic errors on CP-asymmetry parameters. Errors for ϕK^0 and $f_0 K^0$ CP-parameters are based on the low-K^+K^--mass sample. The $K^+K^-K^0$ column refers to errors on average CP parameters across the Dalitz plot.

In the fit to low K^+ K^- masses, we extract CP asymmetry parameters for ϕK^0 and $f_0 K^0$ decays together with isobar parameters for the ϕK^0, while all other isobar parameters are fixed. We evaluate the impact of the fixed parameters on the CP violation results using samples of simulated events. We compare the reference fit result with the fit that has fixed Dalitz parameters smeared by their errors which are taken from Table 1. The average difference in the CP violation parameters is taken as the systematic error. We also assign an error due to uncertainty in the resonant and non-resonant line-shape parameters. For resonant components this includes the uncertainity in the mass and width of the $X_0(1550)$. For that resonance, we replace our nominal parameters with those found by different measurements: $m_r = 1.491$ GeV/c^2, $\Gamma = 0.145$ GeV [17], and $m_r = 1.507$ GeV/c^2, $\Gamma = 0.109$ GeV [2]. We take the largest observed difference from the reference fit as the systematic error. The non-resonant distributions are not motivated by theory so we try several alternative non-resonant models which omit some of the dependences on $K^+K^0_S$ and $K^-K^0_S$ masses (see Eq. 9): $e^{-\alpha m^2_{12}}$, $e^{-\alpha m^2_{12}} + c_{23}e^{i\phi_{23}}e^{-\alpha m^2_{23}}$, and $e^{-\alpha m^2_{12}} + c_{13}e^{i\phi_{13}}e^{-\alpha m^2_{13}}$. We also study the effect of the uncertainty of the shape parameter α on the CP parameters. The non-resonant events contribute to the background under the ϕ but their shape is determined from the high-mass region. We therefore omit the non-resonant terms and re-do the low-mass fits, and take the largest difference from the reference fit as a systematic error. In the full Dalitz plot fit, the non-resonant term is the dominant contribution to the sample and its omission is not reasonable. The mass resolution is neglected in the reference fit since it is small compared to the resonant width for all Dalitz plot components. We evaluate a potential bias on CP-asymmetry parameters by repeating the fit with the Dalitz plot PDF convolved with the mass resolution function and take the difference in the CP parameters into the systematic error.

In the fit to the charge asymmetry in $B^+ \to \phi K^+$ we consider systematic errors due to charge asymmetries in tracking and particle identification (0.011), uncertainties in the parameterization of the signal Fisher PDF (0.003) and B background content (0.012). We add these contributions in quadrature to obtain the total systematic uncertainty on the direct CP violation.

6 CONCLUSIONS

In a fit to $B^0 \to K^+K^-K^0_S(\pi^+\pi^-)$ decays, we analyze the Dalitz plot distribution and measure the fractions to intermediate states, given in Table 1. Subsequently, we extract *CP*-asymmetry parameters from simultaneous fits to $K^+K^-K^0$ final states with the neutral kaon reconstructed as $K^0_S \to \pi^+\pi^-, K^0_S \to \pi^0\pi^0$, or K^0_L. We further analyze the K^+K^- phase-space by computing moments of Legendre polynomials in ϕK^+ and $K^+K^-K^0_S(\pi^+\pi^-)$ decays. We find the P-wave fraction to be 0.29 ± 0.03 averaged over the Dalitz plot, and 0.89 ± 0.01 over the $\phi(1020)$ resonance region ($1.0045 < m_{K^+K^-} < 1.0345$ GeV/c^2).

From a fit to events at low K^+K^- masses, we find $\beta_{\mathit{eff}} = 0.06 \pm 0.16 \pm 0.05$ for $B^0 \to \phi K^0$ and $0.18 \pm 0.19 \pm 0.04$ for $B^0 \to f_0 K^0$, consistent with our previous measurements [9] and with an update of the previous method to the present dataset. We do not observe any significant deviation of *CP* parameters from the Standard Model values $\beta \simeq 0.37, A_{CP} = 0$.

In a fit to the full Dalitz plot, we find the CKM angle $\beta_{\mathit{eff}} = 0.361 \pm 0.079 \pm 0.037$ to be compatible with the SM expectation. Additionally, we resolve the trigonometric ambiguity in the measurement of β_{eff} at 4.6 standard deviations, which is the first such measurement in penguin decays.

7 ACKNOWLEDGMENTS

We are grateful for the extraordinary contributions of our PEP-II colleagues in achieving the excellent luminosity and machine conditions that have made this work possible. The success of this project also relies critically on the expertise and dedication of the computing organizations that support *BABAR*. The collaborating institutions wish to thank SLAC for its support and the kind hospitality extended to them. This work is supported by the US Department of Energy and National Science Foundation, the Natural Sciences and Engineering Research Council (Canada), Institute of High Energy Physics (China), the Commissariat à l'Energie Atomique and Institut National de Physique Nucléaire et de Physique des Particules (France), the Bundesministerium für Bildung und Forschung and Deutsche Forschungsgemeinschaft (Germany), the Istituto Nazionale di Fisica Nucleare (Italy), the Foundation for Fundamental Research on Matter (The Netherlands), the Research Council of Norway, the Ministry of Science and Technology of the Russian Federation, Ministerio de Educación y Ciencia (Spain), and the Particle Physics and Astronomy Research Council (United Kingdom). Individuals have received support from the Marie-Curie IEF program (European Union) and the A. P. Sloan Foundation.

References

[1] Unless explictly stated, charge conjugate is implied throughout this paper.

[2] S. Eidelman *et al.* [Particle Data Group], Phys. Lett. B **592**, 1 (2004).

[3] M. Beneke, Phys. Lett. B **620**, 143 (2005) [arXiv:hep-ph/0505075].

[4] G. Buchalla, G. Hiller, Y. Nir and G. Raz, JHEP **0509**, 074 (2005) [arXiv:hep-ph/0503151].

[5] H. Y. Cheng, C. K. Chua and A. Soni, Phys. Rev. D **72**, 094003 (2005) [arXiv:hep-ph/0506268].

[6] B. Aubert *et al.* [BABAR Collaboration], Phys. Rev. Lett. **94**, 161803 (2005) [arXiv:hep-ex/0408127].

[7] K. Abe *et al.* [Belle Collaboration], [arXiv:hep-ex/0507037].

[8] P. Krokovny, [arXiv:hep-ex/0605023].

[9] B. Aubert *et al.* [BABAR Collaboration], Phys. Rev. D **71**, 091102 (2005) [arXiv:hep-ex/0502019].

[10] B. Aubert *et al.* [BABAR Collaboration], Nucl. Instrum. Meth. A **479**, 1 (2002) [arXiv:hep-ex/0105044].

[11] M. Pivk and F. R. Le Diberder, Nucl. Instrum. Meth. A **555**, 356 (2005) [arXiv:physics/0402083].

[12] B. P. Roe, H. J. Yang, J. Zhu, Y. Liu, I. Stancu and G. McGregor, Nucl. Instrum. Meth. A **543**, 577 (2005) [arXiv:physics/0408124].

[13] H. J. Yang, B. P. Roe and J. Zhu, Nucl. Instrum. Meth. A **555**, 370 (2005) [arXiv:physics/0508045].

[14] H. Albrecht *et al.* [ARGUS Collaboration], Z. Phys. C **48**, 543 (1990).

[15] J. M. Blatt, V. F. Weisskopf, "Theoretical Nuclear Physics", John Wiley & Sons, New York (1952).

[16] C. Zemach, Phys. Rev. **133**, B1201 (1964).

[17] A. Garmash *et al.* [BELLE Collaboration], Phys. Rev. D **71**, 092003 (2005) [arXiv:hep-ex/0412066].

[18] B. Aubert *et al.* [BABAR Collaboration], [arXiv:hep-ex/0605003].

[19] B. Aubert *et al.* [BABAR Collaboration], [arXiv:hep-ex/0507094].

[20] P. Minkowski and W. Ochs, Eur. Phys. J. C **39**, 71 (2005) [arXiv:hep-ph/0404194].

[21] M. Ablikim *et al.* [BES Collaboration], Phys. Lett. B **607**, 243 (2005) [arXiv:hep-ex/0411001].

[22] H. Y. Cheng and K. C. Yang, Phys. Rev. D **66**, 054015 (2002) [arXiv:hep-ph/0205133].

[23] S. Fajfer, T. N. Pham and A. Prapotnik, Phys. Rev. D **70**, 034033 (2004) [arXiv:hep-ph/0405065].

[24] M. Gronau and J. L. Rosner, Phys. Rev. D **72**, 094031 (2005) [arXiv:hep-ph/0509155].

[25] B. Aubert *et al.* [BABAR Collaboration], Phys. Rev. D **72**, 072003 (2005) [arXiv:hep-ex/0507004].

[26] O. Long, M. Baak, R. Cahn, and D. Kirkby, Phys. Rev. D **68**, 034010 (2003).